Mercury shows no immediate affects on F-actin to G-actin ratio in primary culture chick sympathetic neurons.

Blair Rossetti

8 April 2008

Neurobiology

Dr. Robert L. Morris

INTRODUCTION

The cytoskeleton is the dynamic structural bases for all eukaryotic cells. Generally, the molecular building blocks of cytoskeletal filaments include microtubule monomers, called tubulin, and microfilament monomers, called actin, undergo a cyclical pattern of assembly into rod-like structures followed by subsequent disassembly. The constant polymerization and depolymerization of these filamentous structures can provide cells with internal pathways for molecular motor proteins or finger-like cellular extensions with a wide variety of functions. In neurons, cytoskeletal proteins are not only important for defining their unique cellular shape but microtubules and microfilaments are primarily responsible for the outgrowth of neural processes (Kandel et al., 2000).

At the tip of all neuronal extensions is a region known as the growth cone. This area of the cellular process is responsible for directing neurite extensions towards a target cell or region (Leong et al., 2000). A large portion of the growth cone is shaped by filaments of actin and tubulin molecules (Leong et al., 200). Microfilaments are responsible for forming the finger-like regions of the growth cone, called filapodia, that direct the neurite process; whereas, microtubules provide the primary support for the entire growth region (Kandel et al., 2000). Since the neurite process must locate target cells and regions, growth cone components are particularly sensitive to environmental factors (Leong et al., 2000). The sensitivity of the growth cone region can have profound implications when toxic chemicals are introduced to the environment. In particular, evidence has been found supporting mercury's neural degenerative properties (Leong et al., 2000). Mercury has been found to disrupt microtubule polymerization by competing for GTP binding site on tubulin dimers (Leong et al., 2000). Inhibition of tubulin assembly cripples the primary support structure of the neurite extension, leading to retrograde degeneration of the neuronal process.

Due to the withdrawal of the neurite extension as a result of inhibited tubulin polymerization, it is difficult to determine if mercury exposure also impacts the polymerization of actin. Analysis of polymerized actin, called F-actin, and depolymerized actin, called G-actin, ratios after immediate mercury exposure may reveal previously undetectable

effects of mercury on actin assembly. The dependence of F-actin and G-actin quantities on cell size will be normalized in this experiment by comparing the ratio of F- to G-actin. Specifically, the F- to G-actin ratio indicates the amount of F-actin per G-actin molecule. An increase in the F- to G-actin ratio is equivalent to an increase in F-actin and/or a decrease in G-actin. A decrease in the F- to G-actin ratio is equivalent to a decrease in F-actin and/or an increase in G-actin. In this study, we tested the hypothesis that the F-actin to G-actin ratio in primary embryonic sympathetic chick neurons will be lower in mercury treated neurons than in non-mercury treated, control neurons. We believe that F- to G-actin ratio will be lower in mercury treated neurons than in non-mercury treated neurons because we expect mercury to disrupt the polymerization of G-actin to F-actin. Given that mercury's toxic affects on neurons show significant correlation to conditions such as Alzheimer's disease (Leong et al., 2000), a better understanding of the toxicity of mercury may prove to be an invaluable tool in the fight against degenerative neural disease. By understanding how mercury changes or maintains actin dynamics, there is a possibility to gain insight into general response of actin to toxic substances.

To test the aforementioned hypothesis, neurons were dissected from chick, *Gallus gallus*, embryos and treated with 0nM mercury chloride or 100nM mercury chloride. Subsequently, the amount of F-actin and G-actin was indirectly measured by determining the amount of F- and G-actin fluorescent labels. Alexa Fluor 568 phalloidin was used to label F-actin; whereas, Deoxyribonuclease I, Alexa Fluor 488 conjugate was used to label G-actin. Each fluorescent label was specifically chosen to reduce spectral bleed-through during fluorescent imaging. The neurons were obtained from *G. gallus* because it is well studied and widely used as a model organism for neuronal experimentation. The chick embryos have proven to be amenable to experiments involving the dissection and isolation of sympathetic chain and dorsal root ganglia (Morris et al., 1993).

This project was conducted in collaboration with three other researchers enrolled in Neurobiology (Bio 324) at Wheaton College, MA—Michael Grimaldi, Michael Ophir, and Amanda Rawson. All collaborating researchers took part in producing data for this publication; however, they have all completed individual analysis on the pooled data. Michael Grimaldi studied F-actin levels in neurons; Michael Ophir studied F-actin levels in glia; and Amanda Rawson studies F-actin to G-actin ratio in glia. Together, we hope to gain a better understanding of the toxic effects of mercury on actin polymerization.

MATERIALS AND METHODS

Materials

All tissue culture products were obtained from Sigma Chemical Co. (St Louis, MO) unless otherwise noted. Chick embryos were obtained from Charles River SPAFAS Inc. Deoxyribonuclease I, Alexa Fluor 488 conjugate and Alexa Fluor 568 phalloidin were obtained from Invitrogen Corp. Mercury solutions were prepared and provided by Dr. Jani Benoit, Wheaton College MA.

Preparation of buffers

Buffer preparation procedures have been modified from previously stated methods (Jeffery, 2006). Phosphate Buffered Saline (PBS) was made in a 1L portion and contained the following: ~1L distilled H_2O, 80g (8%) NaCl, 2g (0.2%) KCl, 26.8g (2.68%) K_2HPO_4, 2.4g (0.24%) KH_2PO_4. PBS was adjusted to pH 7.4 with 1M HCl or NaOH and filtered into a sterile container. Fixation/Permeabilization Buffer (Fix/Perm) was prepared with the following ingredients: 30mL Liebovitz L-15, 1.62mL (5.4%) 37% formaldehyde, 0.12mL (0.4%) 25% gluteraldehyde, 1.2g (4.0%) sucrose, 0.6mL (2.0%) 25% Triton X-100, and 0.3mL (1.0%) 0.2M EGTA. Fixation Buffer (Fix) was prepared with the following ingredients: 30mL Liebovitz L-15, 1.62mL (5.4%) 37% formaldehyde, 0.12mL (0.4%) 25% gluteraldehyde, 1.2g (4.0%) sucrose, and 0.3mL (1.0%) 0.2M EGTA. Both Fix/Perm and Fix were adjusted to pH ~7 with 1M HCl or 1M NaOH. PBS/Triton X-100 contained the following ingredients: 500mL PBS and 2.5mL (0.5%) 100% Triton X-100. Block Buffer consisted of the following ingredients: 50mL PBS and 1.5g (3.0%) BSA.

Primary tissue culture of chick embryonic sympathetic neurons

Sympathetic chain and dorsal root ganglia were dissected from 9- to 11-day chick embryos as previously described (Morris et al.,1993). Cells were dissociated with incubation at 37°C in trypsin (Ca- and Mg-free HBSS and 0.25% trypsin) for 15-20 minutes. Dissociated cells were plated on poly-L-lysine and laminin treated coverslips in Petri dishes containing 2mL of growth medium (100mL L-15, 2mM glutamine, 0.6% glucose, 100U,ug/mL pen/strep, 10% fetal bovine serum (FBS), and 50ng/mL rat nerve growth factor (NGF)). Incubation on poly-L-lysine treated coverslips ranged from 1-24 hours; whereas, incubation on laminin treated coverslips ranged from 1-16 hours. Plated cells were incubated at 37°C in a humid environment for 1-24 hours before mercury treatment. All cultured chick embryonic sympathetic neurons were provided by Dr. Robert L. Morris, Wheaton College, MA.

Preparation of neurons

Neuron preparation procedures have been modified from previously stated methods (Jeffery, 2006). After the 1-24 hour incubation period, growth medium was removed from the Petri dishes and plated cells were each washed three times with 2mL of Hank's Balanced Salt Solution (HBSS). In this experiment, there was one negative control coverslip, three positive control coverslips, one negative experimental coverslip, and four positive experimental coverslips. All control cells were treated with 2mL of 100nM HCl in HBSS; whereas, all experimental cells were treated with 2mL of 100nM HgCl in HBSS. Both control and experimental cells were incubated at 37°C for 20 minutes. Upon completion of the 20-minute exposure period, all cells were washed three times with 2mL of 37°C HBSS.

Following the washes and removal of HBSS, cells were fixed by adding 2mL of Fix/Perm and incubated at room temperature for 15 minutes. Subsequently, Fix/Perm was removed and the cells were treated with 2mL of Fix and incubated at room temperature for 15 minutes. After the 15-minute exposure period, Fix was removed and cells were washed three times with 2mL of PBS/Triton X-100. Cells were blocked by adding 2mL of Block Buffer and incubated at room temperature for 20 minutes. Once cells were blocked, the Block Buffer was removed and the cells were wash three times with 2mL of PBS.

The PBS washed cells were placed cell-side upwards on coverslip pedestals within a humidity chamber (Fig. 1). In a dark environment, the cell side of the negative control and negative experimental coverslips were treated with 200uL of PBS and the cell side of each positive control and positive experimental coverslip was treated with 200uL of F- and G-actin labeling solution (3.6uL 5mg/mL Deoxyribonuclease I Alexa Fluor 488 conjugate, 50ul 200U/mL Alexa Fluor 568 phalloidin, and 2mL PBS). All coverslips were incubated at room temperature for 20 minutes in a dark environment after treatment. Coverslips were removed from the humidity chamber after the 20-minute fluorescent labeling period. The majority of the labeling solution was removed from the coverslips using a Kimwipe while being sure not to dry out the neurons. The coverslips were replaced into their respective Petri dishes and washed three times with 2mL of PBS. All coverslips were mounted on Gold Seal Micro Slides and sealed with nail polish. Each slide was labeled and stored in a light-tight slide box at -20°C for up to one day or until imaged.

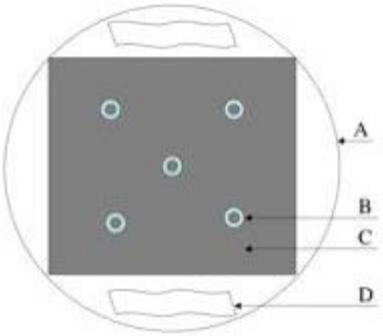

Fig. 1. Humidity chamber containing coverslip pedestals. (A) Large Petri dish. (B) Coverslip pedestal fabricated from eppendorf tube caps. (C) Sheet of parafilm. (D) Kimwipe soaked in water. Each humidity chamber includes an opaque cover.

Standardization of CCD camera

To obtain a curve of exposure versus mean image grayscale value, a thin layer of nail polish painted on a Gold Seal Micro Slide was used as a reference for experimental images. At three distinct areas of nail polish, a range of exposures was taken for the red and green channels. Each range of exposures included an underexposed and an overexposed image. All standardization images were acquired on a Nikon 80*i* Eclipse equipped with a SPOT RT Color CCD camera from Diagnostic Instruments, Inc. on a 0.75x C-mount, EXFO X-Cite 120 Fluorescence Illumination System, Uniblitz Model VMM-D1 Shutter Driver from Vincent Associates, and a Nikon Plan Fluor 40x/0.75 Ph2 DLL. The Nikon 80*i* Eclipse was interfaced with a Power Mac G4 Model Number M8493. To obtain red channel images, a Nikon G-2E/C filter cube was placed in the light path. To obtain green channel images, a Nikon B-2E/C filter cube was placed in the light path. To decrease noise from mercury lamp intensity fluctuation, all images were taken in one sitting. Images at 29 different exposure times ranging from 5ms to 600ms were captured for the red channel and 34 different exposure times ranging from 0.2s to 30s were captured for the green channel. The mean grayscale value for each acquired image was determined by using the Histogram function in ImageJ (v.1.32j).

Phase and fluorescence microscopy

All phase and fluorescence images were acquired on a Nikon 80*i* Eclipse equipped with a SPOT RT Color CCD camera from Diagnostic Instruments, Inc. on a 0.75x C-mount, EXFO X-Cite 120 Fluorescence Illumination System, Uniblitz Model VMM-D1 Shutter Driver from Vincent Associates, and a Nikon Plan Fluor 40x/0.75 Ph2 DLL. The Nikon 80*i* Eclipse was interfaced with a Power Mac G4 Model Number M8493. During image acquisition, all filters and analyzers were removed from the light path.

To locate neurons, each slide was scanned in a raster motion using phase contrast (Ph2). When a neuron was located, the light path was redirected from the oculars to the SPOT RT Color CCD camera. Using the Live function on SPOT (v.4.1.3), the region of interest (ROI) was focused and adjusted for Kohler Illumination. A phase image was acquired using automatic exposure setting. Subsequently, the transmitted illumination source was covered, a Nikon B-2E/C filter cube was placed in the light path, and a green channel (Alex Fluor 568 phalloidin) image was acquired under the following settings: 4.5 second exposure, gain 4, and 24 Bits per Pixel (RGB). After acquisition of a green channel image, a Nikon G-2E/C filter cube was placed in the light path, and a red channel (Deoxyribonuclease I, Alexa Fluor

488 conjugate) image was acquired under the following settings: 0.4 second exposure, gain 4, and 24 Bits per Pixel (RGB). All images were saved as uncompressed tagged image file format (TIFF).

Quantification of data

The following quantification method was developed in collaboration with Michael Grimaldi, Michael Ophir, and Amanda Rawson. All images were processed using ImageJ (v.1.32j). To create a mask for defining the area of quantization, the red channel was first opened in the ImageJ software. Using the Subtract Background function with a Rolling Ball Radius of 50 and White Background selected, the neuron boundaries were defined and the background was converted to white (background grayscale value of 255). The resulting image was then converted to black and white by using the Threshold function under the Binary menu. This mask image was subsequently added to an unmodified version of the red channel image using the Image Calculator function. After selecting the ROI isolating the neuron, a list of grayscale values and counts were obtained from the Copy feature on the Histogram function. The grayscale value and count list was pasted into Excel and a mean grayscale value was calculated excluding grayscale values equal to 255. By removing all grayscale values corresponding to 255, the average is only calculated for pixels from cellular regions and excludes coverslip background pixels. Once a mean grayscale value was calculated for the red channel, the mask was added to an unmodified version of the green channel image using the Image Calculator Function. A mean grayscale value for the green channel was obtained a previously described for the red channel. A ratio of F-actin to G-actin mean grayscale value was obtained by dividing the mean F-actin grayscale value by the mean G-actin grayscale value. All ratios were averaged to determine the average mean F-actin grayscale value to mean G-actin grayscale value ratio.

RESULTS

Exposure time standard curves

Given that mean brightness level is a function of exposure time, an exposure time standard curve was generated in order to quantitatively compare the mean brightness level of fluorescent images. Three distinct areas of nail polish were utilized for the standard curve analysis (Fig. 2). Observations of the trends within the exposure time standard curves are necessary for aiding in the determination of standard red and green channel exposure times to be used for all experimental images. The standard red and green channel exposure times must exist in an exposure time range where different mean brightness levels are distinctly separated. Analysis of the exposure time standard curves indicated that

there are no observed overlaps between the mean brightness level at any given exposure time above 5ms for the red channel and 4s for the green channel. Both the red and green channel standard exposure curves exhibit slight logistic curvature; however, this feature is more pronounces in the green channel (Fig. 3). Since the red channel standard exposure curve is based on a shorter scale of exposure times, the local linearity of the logistic curve is more distinct than the curvature found in the green channel standard exposure curve.

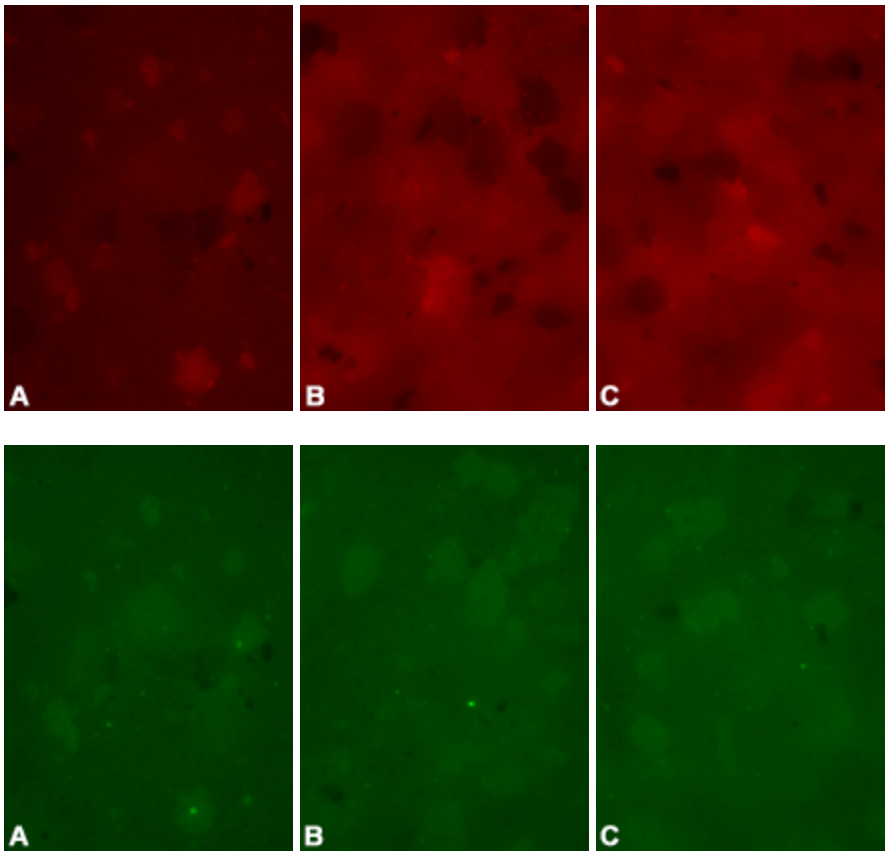

Fig. 2. A subset of the three discrete red channel and green channel images acquired at the same exposure time. (A) Image 1. (B) Image 2. (C) Image 3. All displayed red channel images were acquired at an exposure time of 300ms. All displayed green channel images were acquired at an exposure time of 10s.

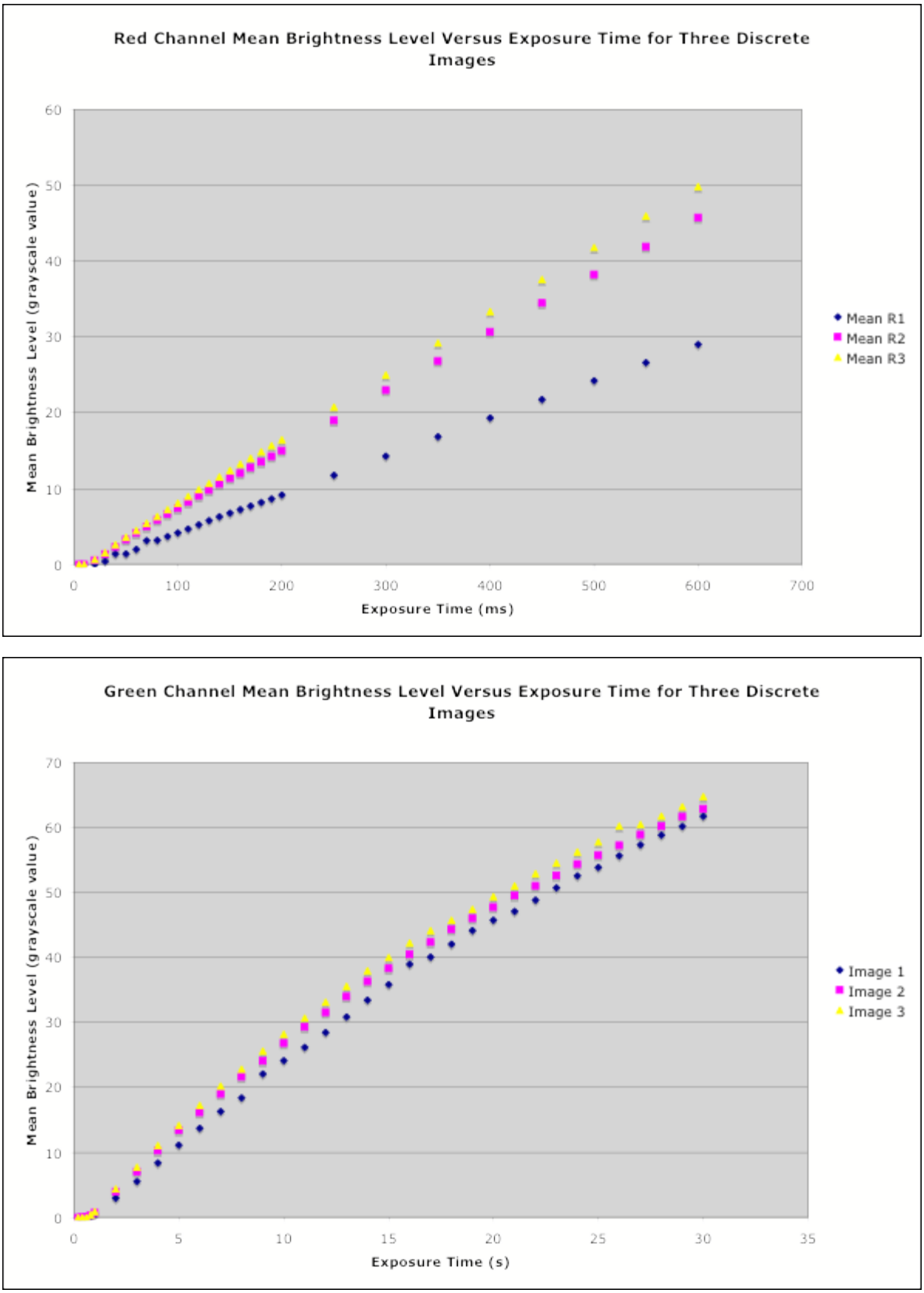

Fig. 3. Exposure time standard curves for red and green channel for three discrete images. Both exposure time standard curves exhibit slight logistic curvature. There was no observed overlap between the mean brightness levels for the red or green channel at any given exposure time. There were 29 different exposure times ranging from 5ms to 600ms for the red channel and 34 different exposure times ranging from 0.2s to 30s for the green channel.

Analysis of average F-actin to G-actin ratio

Red channel images of Alexa Fluor 568 phalloidin were utilized to indirectly locate and quantify the amount of F-actin in any given neuron. Green channel images of Deoxyribonuclease I, Alexa Fluor 488 conjugate were utilized to indirectly locate and quantify the amount of G-actin in any given neuron (Fig. 4). An observation of the negative control and negative experimental slides in both the red and green channels yielded images containing no pixels above background level. By quantifying the mean brightness level for each channel within the boundaries of a neuron, we were able to indirectly measure the amount of F- and G-actin within the neuron. These mean brightness levels were converted into a ratio of mean F-actin brightness level to mean G-actin brightness level in order to nullify the impact of varying cell area on the reported actin levels. In all cases, the neuron boundaries were defined by the masking method described in the Materials and Methods section. Overall, 26 control neurons were analyzed for F- to G-actin ratio and 25 experimental neurons were analyzed for F- to G-actin ratio (Fig. 5).

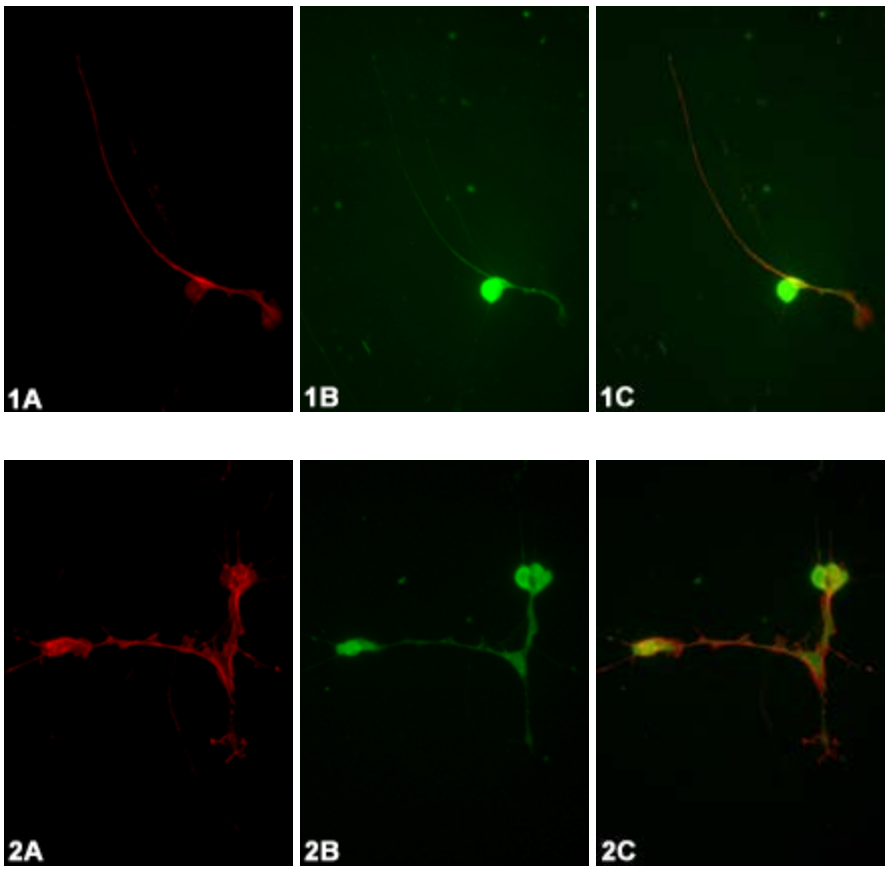

Fig. 4. Alexa Fluor 568 phalloidin, Deoxyribonuclease I Alexa Fluor 488 conjugate, and merged images of control neuron treated with 0nM HgCl (1A, B, and C) and experimental neuron treated with 100nM HgCl (2A, B, and C). (A) Alexa Fluor 568 phalloidin. (B) Deoxyribonuclease I Alexa Fluor 488 conjugate. (C) A and B merged image.

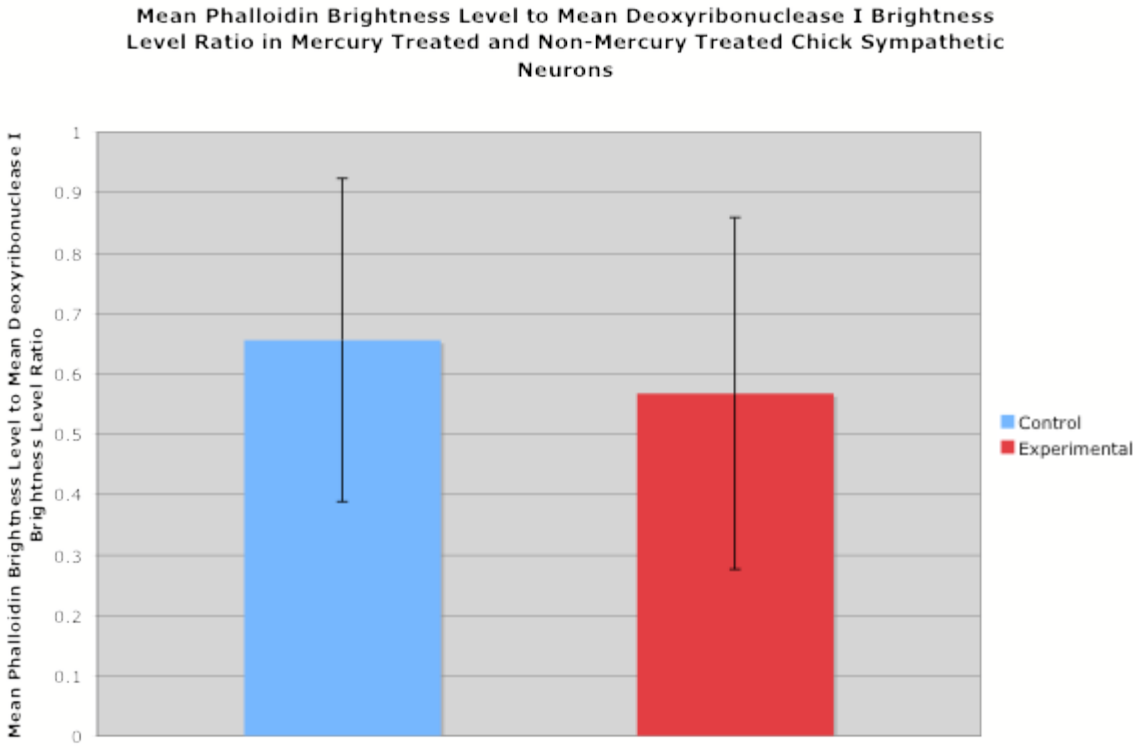

Fig. 5. Graph of the mean Alexa Fluor 568 phalloidin brightness level to mean Deoxyribonuclease I Alexa Fluor 488 conjugate brightness level ratio for control and experimental neurons.

As observed in Figure 5, the mean Alexa Fluor 568 phalloidin brightness level to mean Deoxyribonuclease I Alexa Fluor 488 conjugate brightness level ratios were not significantly different between the mercury treated and non-mercury treated neurons.

DISCUSSION

Mercury shows no immediate affect on F-actin to G-actin ratios

In this study, we have refuted the aforementioned hypothesis by showing that F-actin to G-actin ratios are not immediately affected by mercury exposure. Although the F-actin to G-actin ratio was observed to be lower in the experimental neurons than control neurons, the standard deviation of the average ratios reveals that any difference found between the average ratios was not statistically significant. Since the negative control and negative experiment neurons yielded images without pixels above background, there is no evidence of additional fluorescing compounds contaminating the slides. The negative control and experimental data suggests that any measured brightness level of the positive control and experimental neurons is an accurate measurement of the amount of each fluorescent label and that external factors, such as mercury, are not contributing to the observed brightness levels.

If this experiment were to be repeated and a similar difference was found between the F- and G-actin ratios of the control and experimental neurons, there would be stronger evidence suggesting that mercury causes immediate

depolymerization of F-actin in neurons. In such a case, we could speculate that mercury exposure disrupts the polymerization of actin by inhibiting or altering the conformation of key molecules. A mechanism such as this may be similar to mercury's polymerization inhibiting affect on tubulin molecules. As described by Leong, et al. (2000), mercury vapor inhibits the binding of GTP to b-tubulin, a required stage in the process of tubulin polymerization. Since actin polymerization is modulated by a group of GTPases, specifically Cdc42, Rac, and Rho, mercury may have a similar impact on actin as it does on microtubules (Tanaka et al., 1995). For example, mercury could inhibit the binding of GTP to Cdc42, Rac, or Rho subsequently inhibiting the polymerization of actin.

There were a few particular sources of error in this experiment. The greatest source of error arose from the data quantification process. Due to the method of neuron boundary definition we developed in this experiment, all pixels with a brightness level equal to 255 in the original image are removed from the calculated average. If any pixels of the cellular region are not below 255, the averaging process will delete or remove them. Considering that these brightest pixels carry the largest weight when averaged, they are the most important pixels in the image. In general, the images used in this process were all below 255.

Another source of error in this experiment concerns the imaging process. Since it is not feasible to image every neuron, the selection of which neurons to image can become subjective. By introducing subjectivity into the dataset, there is a possibility to skew the results. If this experiment were to be repeated, there are a few changes that could be made to reduce the sources of error. In particular, the neuron selection for imaging could be based on a randomized system. For instance, images could be taken for every other field of view containing neurons. In addition to the subjectivity on imaging, there is also a great amount of inaccuracies derived from quantifying the brightness of an image. Since fluorophores degrade over time, the neurons get dimmer after every exposure to light. To decrease photobleaching, antifading agents can be added to the procedure. If this experiment were to be repeated, there are a few changes that could be made to reduce the sources of error. In particular, the neuron selection for imaging could be based on a randomized system. For instance, images could be taken for every other field of view containing neurons.

Standard exposure curves indicate separation among mean grayscale values at a given exposure time

In this study, exposure time standard curves were acquired for the green and red channels. Both channels exhibit slight logistic curvature. One explanation of this logistic curvature can be found by observing the nature of mean values. Since an image has a maximum value of 255, there is an upper bound to the exposure curve. As an image gets brighter or as more pixels reach a value of 255, the mean brightness does not receive as much weight towards the higher

brightness levels. This decreases the rate at which the mean brightness increases. A similar explanation can be applied to the lower bound of the exposure curve since an image has a minimum value of 0. As an image gets darker or as more pixels reach a value of 0, the mean brightness does not receive as much weight towards the lower brightness levels. This decreases the rate at which the mean brightness decreases.

One of the most important aspects of the exposure time standard curves is the fact that at mid-range exposures, or exposures that are not completely under or overexposed, contain no intersections of the trend lines. This implies that, for any given mid-range exposure time, the mean brightness level of two or more images can be definitively compared. If an intersection of the trend lines was observed at a particular exposure, these findings would indicated that the relationship between mean brightness levels of two or more images does not remain constant at every exposure time suggesting that the data cannot be definitively compared.

Future experiments

In the future, we would like to reexamine the F-actin to G-actin ratios by utilizing a different quantification technique. We propose replacing the mean brightness level measurements with total brightness level measurements. Since counts of brightness levels are not weights towards brighter values as are the average brightness levels, there may be a greater potential for observing differences in F- to G-actin ratios. We propose increasing the sample size to 50 neurons. The aforementioned dataset would lend well to a more rigorous statistical analysis of F- to G-actin ratios.

The author thanks Dr. Robert L. Morris for his time and guidance throughout the project, Dr. Thomas Ratliff and Dr. Michael Kahn for statistical consultation, Dr. Geoff Collins for image standardizing techniques, and Alison Mehlhorn for laboratory assistance. The author specially thanks the RAMMBA Actin Team (Michael Grimaldi, Michael Ophir, Amanda Rawson, Reed Hollett, and Ashley Furr) for all their hard work and collaboration. This work was supported by the Wheaton College Provost's Office and was accomplished using equipment funded by a grant from the National Science Foundation (grant #0126637).

REFERENCES

Akisaka, T., Yoshida, H., Inoue, S. and Shimizu, K. (2001). Organization of cytoskeletal F-actin, G-actin, and gelsolin in the adhesion structures in cultured osteoclast. *J. of Bone and Mineral Research* **16,** 1248-1255.

Jeffery, B. (2006). Mercury disrupts the arrangement of axonal microtubules in primary cultured chick sympathetic neurons. *ICUC Server.*

Kandel, E.R., Schwartz, J.H. and Jessell, T.M. (2000) Principles of Neural Science. 4th ed. New York:McGraw-Hill. 1414 p.

Leong, C.C.W., Syed, N.I. and Lorscheider, F.L. (2000). Retrograde degeneration of neurite membrane structural

integrity of nerve growth cones following *in vitro* exposure to mercury. *NeuroReport* **12,** 733-737.

Morris, R.L. and Hollenbeck, P.J. (1993). The regulation of bidirectional mitochondrial transport is coordinated with axonal outgrowth. *J. of Cell Science* **104,** 917-927.

Paglini, G. Kundam, P., Quiroga, S., Kosik, K. and Caceres, A. (1998). Suppression of radixin and moesin alters growth cone morphology, motility, and process formation in primary cultured neurons. *J. Of Cell Biol.* **143,** 443-455.

Paglini, G. Kundam, P., Quiroga, S., Kosik, K. and Caceres, A. (1998). Suppression of radixin and moesin alters growth cone morphology, motility, and process formation in primary cultured neurons. *J. Of Cell Biol.* **143,** 443-455.

Silverio, A. (2006). Rhodamine phalloidin stain indicates greater amount of actin in mercury-treated primary chick sympathetic neurons. *ICUC Server*.

Tanaka, E. and Sabry, J. (1995). Making the connection: cytoskeletal rearrangements during growth cone guidance. *Cell Press* **83,** 171-176.